Phase stability of boron carbon nitride in a heterographene structure: A first-principles study

AUTHOR(S):

Yuge, Koretaka

CITATION:

Yuge, Koretaka. Phase stability of boron carbon nitride in a heterographene structure: A first-principles study. PHYSICAL REVIEW B 2009, 79(14): 144109.

ISSUE DATE:

2009-04

URL:

http://hdl.handle.net/2433/109869

PHYSICAL REVIEW B **79**, 144109 (2009)

Phase stability of boron carbon nitride in a heterographene structure: A first-principles study

Koretaka Yuge
Department of Materials Science and Engineering, Kyoto University, Sakyo, Kyoto 606-8501, Japan
(Received 26 January 2009; revised manuscript received 12 March 2009; published 8 April 2009)

Phase stability for monolayer boron-carbon-nitride (BNC) (l-BNC) ternary system was examined by Monte Carlo simulations and the cluster expansion technique based on first-principles calculations. All the possible atomic arrangements exhibit positive formation energies, indicating phase separation into monolayer BN and graphene. The atomic arrangements in lowest formation energy have strong preferences for B-N and C-C atoms while disfavor with B-C, C-N, B-B, and N-N bonds along the first-nearest-neighbor coordination, which have a similar tendency for cubic BNC ternary alloys predicted in our previous study. Lattice vibration significantly enhances solubility limits for l-BNC: within the framework of harmonic approximation, complete miscibility achieves at around $T=3500$ K, which is below melting lines between hexagonal BN and graphite.

DOI: 10.1103/PhysRevB.79.144109 PACS number(s): 81.30.−t, 64.70.kg, 64.75.−g

I. INTRODUCTION

Boron-carbon-nitride (BNC) ternary compounds show wide variety of physical properties with their polymorphic structures. The cubic structure, c-BNC, is expected to show outstanding high hardness since c-BN and diamond both have ultrahigh bulk modulus, melting temperature, and high hardness.[1,2] The graphitelike layered structure (hereinafter we write g-BNC) is expected to behave semiconductor with wide variety of band gap, since layered structure of carbon (graphite) and boron-nitride (h-BN) are semimetal and insulator, respectively. Furthermore, the g-BNC is a potential candidate as intercalation material for Li ion batteries.[3,4] Since these properties should be affected by their composition and atomic arrangements, phase stability of the BNC systems can be significantly informative for suitable design of such materials.

Phase stability of the c-BNC has been investigated so far both experimentally[1,2,5–7] and theoretically.[8–10] In the previous works, despite the success of synthesis for the c-BNC, their phase stability including whether c-BNC forms stable intermediate phase or undergoes phase separation into c-BN and diamond was still under discussion. Several theoretical works based on density-functional theory (DFT) supports the tendency of phase separation. Very recently, Yuge *et al.*[11] constructed c-BNC phase diagram through DFT including the effect of lattice vibration and confirmed the quantitative solubility limit, significant vibrational contribution to the solubility, and short-range ordering tendency for the c-BNC.

The g-BNC is fabricated by variety of methods such as chemical vapor deposition, solid-phase pyrolysis, and shock synthesis.[12–19] The resultant layered structure have been carefully investigated. Kaner *et al.*[12] confirmed that graphitelike sheet is a composite of B, C, and N atoms using x ray and electron-diffraction measurement. Kawaguchi[19] suggested a possible atomic arrangement of BC_3N with no B-B and N-N bonds along intralayer through electron spectroscopy for chemical analysis (ESCA). Theoretical approach based on the DFT or semiempirical method has been performed to investigate electronic structure and lattice dynamics for g-BNC.[20–23] The phase stability of g-BNC in monolayer or multilayer is also actively addressed by many theoretical works.[24–27] They elucidated that (i) stable g-BNC phase is formed so as to increase B-N and C-C bonds along intralayer first-nearest-neighbor (1-NN) coordination, (ii) B-B and N-N bonds markedly destabilize the g-BNC, and thus (iii) phase separation into layered BN and C_2 (graphene) is anticipated along the intralayer. These calculations neglected contribution of lattice vibration and investigated the phase stability with limited number of atomic arrangements within a couple of dozen each of which consist of around 8–32 atoms in intralayer. Meanwhile, recent theoretical investigations of metal alloys point out that quantitative estimation of the phase stability typically requires millions of atomic arrangements consisting of typically several hundreds or thousands of atoms, and it should consider the dependence of enthalpy on atomic arrangements and the effect of atomic orderings on configuration entropy.[28–31] Besides, the effect of lattice vibration is expected to play significant role on the phase stability of g-BNC since (i) lattice vibration significantly affects solubility in c-BNC (Ref. 11) and (ii) the vibrational modes for monolayer BC_2N are sensitively affected by local atomic arrangements.[22] With these theoretical considerations, further investigation is required for quantitative assessment of the phase stability of the g-BNC.

In the present work, we examine phase stability of monolayer BNC (hereinafter we write l-BNC) with a composition range of $(BN)_{1-x}(C_2)_x$ $(0\leq x\leq 1)$ that is naturally led from the mixture of l-BN and graphene and address the above issues using the cluster expansion (CE) (Ref. 32) technique based on DFT calculations. Since g-BNC would be characterized by intralayer covalent bonding and weaker interlayer van der Waals interactions, present study on the l-BNC can be a fundamental start for understanding the phase stability of the g-BNC. The atomic-arrangement dependence of total energy is accurately treated through CE technique based on DFT. The resultant effective interactions are applied to the Monte Carlo (MC) simulation to obtain statistical ensemble averages. The effect of lattice vibration on the phase diagram is also considered using the first-principles-based lattice-dynamics calculations.

II. METHODOLOGY

Since details of the present calculation treatment are published elsewhere,[11,29,33,34] we summarize the methodology

briefly below. The CE technique is adopted to expand DFT energies. We consider the Helmholtz free energy of a system with given atomic arrangement $\vec{\sigma}$ at temperature T described as

$$F(\vec{\sigma},T) = E_{\mathrm{el}}(\vec{\sigma}) + F_{\mathrm{vib}}(\vec{\sigma},T), \tag{1}$$

where E_{el} and F_{vib} denote the electronic and vibrational contributions to the free energy. In the present work, we neglect the effects of thermal expansion on the total free energy F. In the CE technique, we define the spin variable $\sigma_i=\{+1,0,-1\}$ that specifies the occupation of B, C, and N atoms at lattice point i on a graphene structure. Using σ_i, we construct the following cluster functions that are complete and orthonormal for whole N lattice points:[11]

$$F(\vec{\sigma},T) = V_0\Phi_0 + \sum_n \sum_{(\tau)} V_n^{(\tau)}(T)\Phi_n^{(\tau)}(\vec{\sigma}),$$

$$\Phi_n^{(\tau)} = \phi_{\tau_1}(\sigma_{n_1})\phi_{\tau_2}(\sigma_{n_2})\cdots\phi_{\tau_n}(\sigma_{n_n}),$$

$$\phi_0(\sigma_i) = 1,$$

$$\phi_1(\sigma_i) = \sqrt{\frac{3}{2}}\sigma_i,$$

$$\phi_2(\sigma_i) = -\sqrt{2}\left(1-\frac{3}{2}\sigma_i^2\right). \tag{2}$$

Here, the expansion coefficient V, called effective cluster interaction (ECI), depends on temperature T due to the temperature dependence of vibrational contribution F_{vib} in Eq. (1). $\phi(\sigma_i)$ is orthonormal basis function for lattice point i. Note that two sets of indices should be required to specify the cluster function Φ: one is a set of lattice sites $\{i,j,\ldots,k\}$, which configure the cluster figure n. Another is a set of index of basis function represented by the subscript of ϕ (τ).

In order to determine the ECIs, we perform least-squares (LS) fitting of the total energies for l-BNC ordered structures obtained via DFT calculations. For electronic contribution E_{el}, we obtain total energies for 307 ordered structures, all consisting of 32 atoms, i.e., a 4×4 expansion of the unit cell in the graphene structure. Brillouin-zone integration is performed on the basis of the Monkhorst-Pack scheme with a 2×2 k-point mesh parallel to the layer and one k-point mesh perpendicular to the layer. Other calculation conditions are described in the previous paper.[11] Due to the limited number of DFT input energies, we should choose optimal set of clusters in the CE and set of ordered structures applied to the DFT calculation. These are determined on the basis of the genetic algorithm to minimize the uncertainty of the energies predicted by ECIs, which is called a cross-validation (CV) score,[35–38] and on the construction of ground-state diagrams.[39] The contribution of lattice vibration, F_{vib}, is treated within the harmonic approximation. We neglect the effects of anharmonic lattice vibration which could not be negligible at high temperatures near melting point: the estimation of anharmonicity is out of our present scope. For the vibrational free-energy estimation, we have performed DFT calculation on 21 structures each of which consists of 128 atoms, i.e., a 8×8 expansion of the unit cell in the graphene structure. The k-point mesh of 2×2 parallel to the layer is employed (i.e., corresponding to 16×16 mesh in Brillouin zone of the unit cell), which is sufficient in terms of k-point dependence of the vibrational free energy. Other calculation condition for the lattice vibration is described in our previous work.[11]

TABLE I. Calculated solution energies ΔE^{sol} (in eV) of neighboring B-N and C-C atoms for l-BNC and c-BNC. Values in parentheses represent solution energies in l-BNC measured from those in c–BNC (Ref. 34).

	l-BNC	c-BNC
C-C	2.02 (−0.67)	2.69
B-N	2.21 (−0.65)	2.86

Combining the CE technique with MC simulation, we can obtain configurational properties of l-BNC. The MC statistical thermodynamic simulations in the canonical and grand-canonical ensembles are carried out on the METROPOLIS algorithm. We used 8×8 expansion of the graphene unit cell under two-dimensional periodic boundary conditions, which is found to be sufficient in terms of the cell-size dependence of the MC results. We employ other calculation conditions described in the previous paper.[11]

III. RESULTS AND DISCUSSION

A. Solubility in dilution limit

We first discuss the qualitative trends of solubility for l-BNC in dilution limit. Previous papers[11,34] reveal that (i) c-BNC undergoes phase separation into c-BN and diamond and (ii) the c-BNC solid solution strongly favors neighboring B-N and C-C atoms up to melting temperature. Assuming the similarity of phase stability for l-BNC and c-BNC, we consider a model of dilution limit in l-BNC solid solution where single-neighboring B-N (C-C) atoms solute into bulk graphene (l-BN) in order to investigate a trend of solubility in l-BNC. This model for dilution limit has been applied to c-BNC solid solution and successfully gave qualitative interpretation of pressure effects on c-BNC solubility limits.[34] We performed DFT calculations on 128-atom supercell of graphene (l-BN) where neighboring C-C (B-N) atoms are replaced with B-N (C-C) atoms. The trends of solubility is investigated by introducing solution energy of B-N (C-C) atoms into graphene (l-BN) defined as

$$\Delta E_{\mathrm{BN(CC)}}^{\mathrm{sol}} = E_{\mathrm{BN(CC)}}^{\mathrm{dilute}} - (n_{\mathrm{BN}}E_{\mathrm{l\text{-}BN}} + n_{\mathrm{CC}}E_{\mathrm{graph}}). \tag{3}$$

$E_{\mathrm{BN(CC)}}^{\mathrm{dilute}}$ denotes total energy of dilution limit model for graphene (l-BN) where neighboring C-C (B-N) atoms are replaced with B-N (C-C) atoms described above, $E_{\mathrm{l\text{-}BN}}$ of bulk l-BN, and E_{graph} of bulk graphene. n_{BN} and n_{CC} represent number of B-N and C-C atoms in the dilution limit model, respectively. The resultant solution energies for l-BNC are summarized in Table I together with those for c-BNC.[34] Parentheses denote solution energies in l-BNC measured from those in c-BNC. Solution energies for neigh-

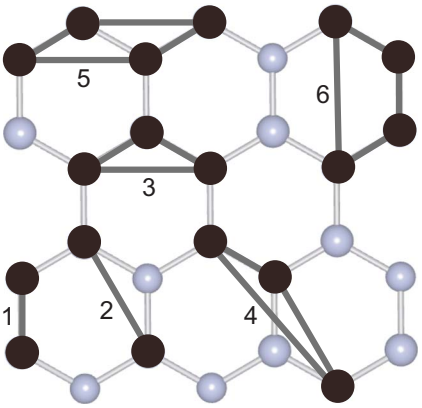

FIG. 1. (Color online) Selected multibody clusters used in the graphene structure.

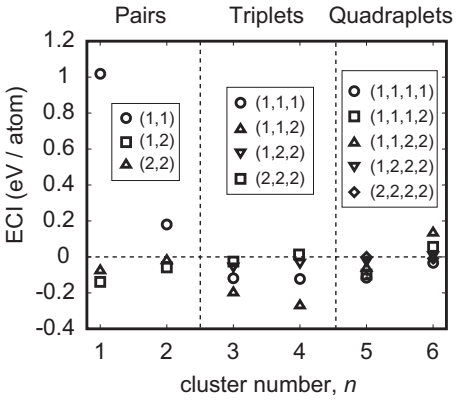

FIG. 2. Effective cluster interactions for the multibody clusters in l-BNC. Parentheses denote basis functions for each lattice point given by Eq. (2).

boring C-C and B-N atoms in l-BNC exhibit positive sign, indicating trends of phase separation into l-BN and graphene. Another notification is that the solution energy for B-N atoms is 0.19 eV larger than that for C-C, which indicates that solubility of B-N into graphene is smaller than that of C-C into l-BN in the dilution limit. This is a similar tendency for c-BNC where solution energy for B-N atoms is 0.17 eV larger than that for C-C. Moreover, solution energies for C-C and B-N atoms in l-BNC are ~0.7 eV smaller than those in c-BNC. Therefore, larger solubility in l-BNC is expected than that in c-BNC. More quantitative estimation of solubility should require accurate treatment of solution energy depending on atomic arrangements and composition in l-BNC, which will be discussed in Secs. III B–III D.

B. Effective cluster interactions for l-BNC

Following the procedure in Sec. II, we finally choose eight clusters consisting of one empty, one point, two pair, two triplet, and two quadruplet clusters; multibody clusters are shown in Fig. 1. These multibody clusters all consist of up to fourth-nearest neighbor pairs, indicating that energetics for l-BNC is well characterized by the local atomic arrangements. The set of clusters exhibits a CV score of 6 meV per atom, where standard deviation of DFT fitted energies is 360 meV per atom. These clusters give sufficient accuracy for expressing relative energetics of individual atomic arrangements in l-BNC. The corresponding ECIs are shown in Fig. 2. We can see the dominant contribution of 1-NN pair cluster (cluster No. 1) with basis function index (1,1). The ECIs for pair cluster appear to converge with respect to the interatomic distances.

While the ECIs for pairs have clear interpretation of coefficients of the orthonormal expansion in Eq. (2), they do not give us intuition of which atomic bonds tend to be preferred. Therefore, we project orthonormal basis functions Φ onto cluster-probability basis functions, which have a transparent interpretation in terms of the ordering tendency. We should note here that since the cluster-probability basis is not orthonormal, we use them just for examining the trends of preference for atomic bonds. The effective interaction based on the cluster-probability basis is called quasibinary effective pair interactions (QEPIs).[40] The QEPI, W, can be obtained by linear combination of ECIs (Ref. 11) and have an explicit form as

$$W_{IJ}^{i} = \tfrac{1}{4}[F_{II} + F_{JJ} - F_{IJ} - F_{JI}], \tag{4}$$

where F_{IJ} denotes the average Helmholtz free energy of all the atomic arrangements in ternary system with I and J atoms in pair cluster i. Therefore, $W_{IJ} > 0$ corresponds to a preference of I-J unlike atom pair with respect to I-I and J-J like atom pairs and $W_{IJ} < 0$ corresponds to a disfavor of I-J atom pair. The resultant QEPIs are shown in Fig. 3. We can clearly see the dominant contribution of the 1-NN pair clusters. Another important notification is that the largest contribution comes from the B-N atoms in the 1-NN coordination $W_{\mathrm{BN}}^{\text{1-NN}}$. Since $W_{\mathrm{BN}}^{\text{1-NN}}$ is in positive sign, neighboring B-N atoms are strongly preferred in l-BNC. The dominant contribution of the neighboring B-N atoms in l-BNC was also seen in the case of c-BNC,[11] which would indicate similar energy dependence of atomic arrangements for l-BNC and c-BNC. Since both h-BN and graphite should have strong preference of neighboring B-N and C-C atoms, the large value in positive sign of $W_{\mathrm{BN}}^{\text{1-NN}}$ suggests phase separation of l-BNC into l-BN and graphene.

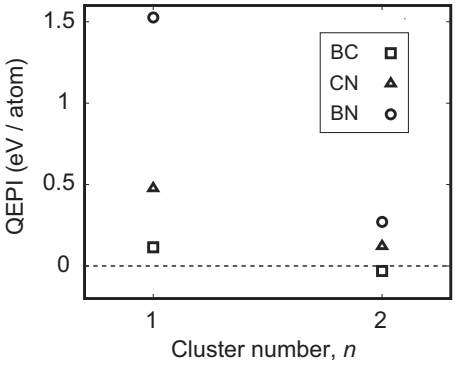

FIG. 3. Quasibinary effective pair interactions for cluster Nos. 1 and 2 in Fig. 1.

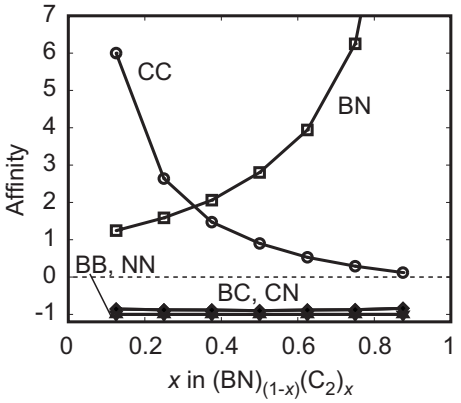

FIG. 4. Calculated affinity α along the 1-NN coordination for the atomic arrangements in lowest formation energy found in MC simulation, as a function of composition x.

C. Ground-state analysis

According to Sec. III B, l-BNC is expected to undergo phase separation since mixture of l-BN and graphene would cause positive energy gain due to the strong preference of neighboring B-N bonds. In this section, quantitative assessment of stable intermediate phase is examined based on the MC simulation with multiple compositions in l-BNC. Since for ternary system, even 8×8 expansion of graphene unit cell have astronomical number of possible atomic arrangements ($\sim10^{61}$), estimation of formation energies for all these arrangements is not practical. In the present work, we perform MC simulation for 128-atom supercell with seven compositions of x ($0.125\leq x\leq0.875$ with composition grid of 0.125) based on simulated annealing algorithm. The initial temperature of the MC simulation box is at $T=100\,000$ K and is gradually decreased by 250 K after 8000 Monte Carlo steps per site until the temperature become 0 K. We found that formation energy for all the possible atomic arrangements exhibit positive sign, indicating that no stable ground-state structures exists and thus l-BNC undergoes phase separation into l-BN and graphene.

While we found that l-BNC is in phase-separating system, at finite temperature a solid solution can be formed. Tendency of which elemental bond is preferred in the l-BNC solid solution can be qualitatively predicted by analyzing the preference of bond for atomic arrangements in lowest formation energy found in the above MC simulation. Due to the use of the finite size of cell, l-BN and graphene are forced to be mixed rather than undergo ideal phase separation. In the present work, the bond preferences in the l-BNC is investigated by affinity α defined as

$$\alpha_n^{IJ}=\frac{y^{IJ}(\text{system})}{y^{IJ}(\text{random})}-1, \tag{5}$$

where y^{IJ}(system) and y^{IJ}(random) represent the pair probability of I-J elements for the system and completely disordered alloy, respectively. Therefore, $\alpha^{IJ}>0$ represents a preference of I-J bond and $\alpha^{IJ}<0$ represents disfavor. Figure 4 shows the resultant simulated affinity along the 1-NN coordination for the atomic arrangements in lowest formation energy in the MC simulation. We can clearly see from Fig. 4 that for all the compositions x, (i) B-N and C-C bonds are strongly favored. (ii) The affinities of B-B and N-N bonds are almost -1, indicating that B-B and N-N bonds are both particularly disfavored in l-BNC. This is consistent with early experimental study by Kawaguchi[19] based on ESCA spectra. (iii) Affinities of B-C and C-N bonds show negative value but are slightly larger than those of B-B and N-N bonds. These preference or disfavor of the 1-NN bonds certainly reflects the tendency of phase separation into l-BN and graphene. The disfavor of B-B, N-N, B-C, and C-N bonds is interpreted by the counterpart of the strong preference of B-N and C-C bonds. These tendencies of the 1-NN bond preferences in l-BNC are consistent with previous theoretical works[25–27] and are also seen in the case of c-BNC,[11] which indicates the similar energy dependence of atomic arrangements along the 1-NN coordination.

D. Phase diagram of l-BNC

From the above discussions, we confirmed that l-BNC has no stable intermediate phase and undergoes phase separation into l-BN and graphene. In this section, we construct the phase diagram using the ECIs and grand-canonical MC simulation. In order to obtain the phase diagram in the grand-canonical MC simulation, we estimate composition x as a function of $\Delta\mu=\mu_{\text{BN}}-\mu_{\text{C}_2}$,[11] where μ_{BN} and μ_{C_2} denote chemical potential of BN and C_2, respectively. During the MC simulation, we perform two types of MC simulation: one is we increase the chemical potential $\Delta\mu$ discretely from -1.00 to 1.80 eV by 0.02 eV and the other is we decrease $\Delta\mu$ from 1.80 to -1.00 eV by -0.02 eV. The resultant $\Delta\mu$-x curve should show a hysteresis between increase and decrease in $\Delta\mu$, because a phase-separating system typically requires driving force for a drastic change in composition due to the phase coexistence, which should correspond to finite excess of chemical potential from the equilibrium state in the grand-canonical MC simulation. We can then estimate the solubility limits from the hysteresis curve, which is described in detail in the previous paper.[11] Errors of the estimated solubility limits due to using the hysteresis curve are within $\pm0.5\%$ of composition throughout the temperature in the present MC simulations.

Applying the simulation on $\Delta\mu$-x curve, we can finally obtain phase diagram of l-BNC as shown in Fig. 5. The broken curve neglects the effect of lattice vibration, and the solid curve includes the effect of lattice vibration. In order to examine the miscibility of l-BNC below the melting point, a hypothetical melting line is drawn together by the broken-dotted line, assuming that the melting point is a linear average of that of h-BN ($T_m\sim3300$ K) (Ref. 41) and of graphite ($T_m\sim4200$ K).[42] For the effect of lattice vibration, we calculate the vibrational free energy for 21 selected atomic arrangements in order to avoid a huge amount of computational effort. These 21 arrangements includes nine atomic arrangements in lowest formation energy found in the MC simulation in Sec. III C, and other 12 arrangements correspond to near the lowest formation energies. Here, the 12 structures are needed to perform the LS fitting because the

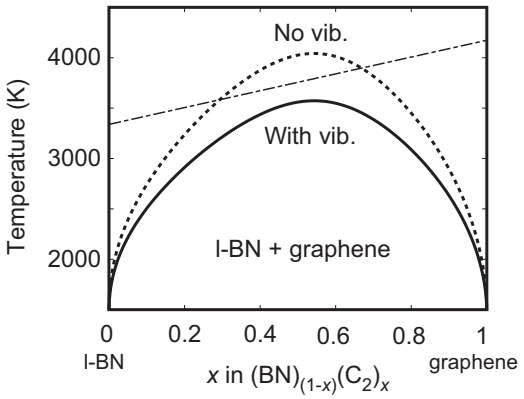

FIG. 5. Calculated phase diagram for c-BNC along the composition range of $(BN)_{1-x}(C_2)_x$ $(0 \leq x \leq 1)$. The broken curve neglects the effect of lattice vibration and the solid curve includes the effect of lattice vibration. The broken-dotted line denotes melting line under an assumption of the linear average of the melting point of h-BN and graphite.

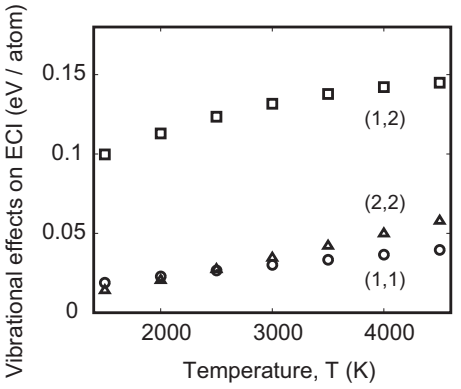

FIG. 6. The effects of lattice vibration on ECIs for the 1-NN pair cluster.

use of nine structures causes linear dependent in cluster functions. The vibrational free energies are expanded up to the 1-NN pair cluster, where the 1-NN spring models can reasonably predict vibrational entropy differences with the accuracy that is one order better than the configurational entropy differences for both metallic and semiconductor systems.[43,44] These clusters give reasonable CV scores below ~10 meV per atom up to the temperature $T=4500$ K. The corresponding vibrational effects on ECIs for the 1-NN pair cluster are shown in Fig. 6 as a function of temperature. Here, we do not show the vibrational effects on QEPIs since they do not give us intuition in terms of the solubility of the l-BNC. We can see from Fig. 5 that at $T=2500$ K and without effects of lattice vibration (dashed line), the solubility limit of ~6.7% for l-BN rich composition is slightly larger than that of ~5% for graphene rich composition, which is consistent with smaller solution energy of C-C atoms in l-BN compared with that of B-N atoms in graphene as shown in Table I. Another important point in Fig. 5 is that within the framework of harmonic approximation, lattice vibration significantly enhances solubility resulting in complete miscibility at around $T=3500$ K which is below the assumed melting temperatures. We should state here that near melting temperature, there still remains possibility of forming more stable phases which have different structure from graphene than solid solution of l-BNC. The significant enhancement of solubility due to lattice vibrational effects is also confirmed in the case of c-BNC,[11] although complete miscibility is around $T=4500$ K, which is above melting temperatures for the c-BNC system. The larger solubility in l-BNC than that in c-BNC is certainly attributed to the smaller solution energies of neighboring C-C and B-N atoms into graphene and l-BN than that into diamond and c-BN, as is described in Table I.

IV. CONCLUSIONS

Phase stability of l-BNC with respect to l-BN and graphene is examined by the combination of cluster expansion technique and Monte Carlo simulation based on first-principles calculations. The solution energies of neighboring B-N and C-C atoms into l-BN and graphene both show positive sign, which supports tendency of phase separation. The solution energies for l-BNC are ~0.7 eV smaller than those for c-BNC, indicating larger solubility in the l-BNC. Estimated ECIs for the l-BNC indicate a strong preference of neighboring B-N atoms, which is a similar tendency found in the c-BNC. We have confirmed that no stable intermediate phase exists between l-BN and graphene through construction of ground-state diagram: formation energies for all the possible atomic arrangements exhibit positive sign. The atomic arrangements in lowest formation energies explicitly show strong preference of neighboring B-N and C-C atoms while B-C and C-N atoms are disfavored. Particularly, no B-B and N-N atoms exist for these atomic arrangements, which is consistent with early experimental study using ESCA spectra. Using the MC statistical simulation on grand-canonical ensemble, l-BNC phase diagram is constructed. We found that within the framework of harmonic approximation, lattice vibration significantly enhances solubility limits of both l-BN and graphene-rich compositions and also decreases critical temperature of complete miscibility at T ~3500 K, which is below assumed linear-average melting line between h-BN and graphite.

ACKNOWLEDGMENTS

The author expresses cordial thanks to Kazuaki Toyoura for fruitful advice in the first-principles calculations.

[1] E. Knittle, R. B. Kaner, R. Jeanloz, and M. L. Cohen, Phys. Rev. B **51**, 12149 (1995).
[2] V. L. Solozhenko, D. Andrault, G. Fiquet, M. Mezouar, and D. C. Rubie, Appl. Phys. Lett. **78**, 1385 (2001).
[3] M. Morita, T. Hanada, H. Tsutsumi, Y. Matsuda, and M. Kawaguchi, J. Electrochem. Soc. **139**, 1227 (1992).
[4] M. Kawaguchi, Y. Imai, and N. Kadowaki, J. Phys. Chem. Solids **67**, 1084 (2006).
[5] A. R. Badzian, Mater. Res. Bull. **16**, 1385 (1981).
[6] S. Nakano, M. Akaishi, T. Sasaki, and S. Yamaoka, Chem. Mater. **6**, 2246 (1994).
[7] T. Komatsu, M. Nomura, Y. Kakudate, and S. Fujisawa, J. Mater. Chem. **6**, 1799 (1996).
[8] W. R. L. Lambrecht and B. Segall, Phys. Rev. B **47**, 9289 (1993).
[9] J. Zheng, C. H. A. Huan, A. T. S. Wee, R. Wang, and Y. Zheng, J. Phys.: Condens. Matter **11**, 927 (1999).
[10] J. C. Zheng, H. Q. Wang, A. T. S. Wee, and C. H. A. Huan, Phys. Rev. B **66**, 092104 (2002).
[11] K. Yuge, A. Seko, Y. Koyama, F. Oba, and I. Tanaka, Phys. Rev. B **77**, 094121 (2008).
[12] R. B. Kaner, J. Kouvetakis, C. E. Warble, M. L. Sattler, and N. Bartlett, Mater. Res. Bull. **22**, 399 (1987).
[13] A. W. Moore, S. L. Strong, G. L. Doll, H. S. Dresselhous, I. L. Spain, C. W. Bowers, J. P. Issi, and L. Piraux, J. Appl. Phys. **65**, 5109 (1989).
[14] M. Kawaguchi, T. Kawashima, and T. Nakajima, Chem. Mater. **8**, 1197 (1996).
[15] M. Hubacek and T. Sato, J. Solid State Chem. **114**, 258 (1995).
[16] L. A. J. Garvie, H. Huvert, P. Rez, P. F. McMillan, and P. R. Buseck, J. Alloys Compd. **290**, 34 (1999).
[17] K. Yamada, J. Am. Ceram. Soc. **81**, 1941 (1998).
[18] J. P. Nicolich, F. Hofer, G. Brey, and R. Riedel, J. Am. Ceram. Soc. **84**, 279 (2001).
[19] M. Kawaguchi, Adv. Mater. (Weinheim, Ger.) **9**, 615 (1997).
[20] A. Y. Liu, R. M. Wentzcovitch, and M. L. Cohen, Phys. Rev. B **39**, 1760 (1989).
[21] Y. Miyamoto, M. L. Cohen, and S. G. Louie, Phys. Rev. B **52**, 14971 (1995).
[22] H. Nozaki and S. Itoh, Phys. Rev. B **53**, 14161 (1996).
[23] Z. Pan, H. Sun, and C. Chen, Phys. Rev. B **73**, 193304 (2006).
[24] P. Saalfrank, W. Rümler, H.-U. Hummel, and J. Ladik, Synth. Met. **52**, 1 (1992).
[25] H. Nozaki and S. Itoh, J. Phys. Chem. Solids **57**, 41 (1996).
[26] S. Azevedo, Eur. Phys. J. B **44**, 203 (2005).
[27] S. Azevedo, Phys. Lett. A **351**, 109 (2006).
[28] A. van de Walle and G. Ceder, Rev. Mod. Phys. **74**, 11 (2002).
[29] K. Yuge, A. Seko, A. Kuwabara, F. Oba, and I. Tanaka, Phys. Rev. B **74**, 174202 (2006).
[30] K. Yuge, A. Seko, I. Tanaka, and S. R. Nishitani, Phys. Rev. B **72**, 174201 (2005).
[31] V. Ozoliņs, C. Wolverton, and A. Zunger, Phys. Rev. B **58**, R5897 (1998).
[32] J. M. Sanchez, F. Ducastelle, and D. Gratias, Physica A **128**, 334 (1984).
[33] K. Yuge, A. Seko, A. Kuwabara, F. Oba, and I. Tanaka, Phys. Rev. B **76**, 045407 (2007).
[34] K. Yuge, J. Phys.: Condens. Matter **21**, 055403 (2009).
[35] M. Stone, J. R. Stat. Soc. Ser. B (Methodol.) **36**, 111 (1974).
[36] D. M. Allen, Technometrics **16**, 125 (1974).
[37] A. van de Walle, M. Asta, and G. Ceder, CALPHAD: Comput. Coupling Phase Diagrams Thermochem. **26**, 539 (2002).
[38] A. van de Walle and M. Asta, Modell. Simul. Mater. Sci. Eng. **10**, 521 (2002).
[39] V. Blum and A. Zunger, Phys. Rev. B **70**, 155108 (2004).
[40] C. Wolverton and D. de Fontaine, Phys. Rev. B **49**, 8627 (1994).
[41] V. L. Solozhenko, in *Properties of Group III Nitrides*, EMIS Data Review Series No. 11, edited by J. H. Edgar (INSPEC/IEE, Stevenage, 1994), pp. 43–70.
[42] F. P. Bundy, Physica A **156**, 169 (1989).
[43] A. van de Walle, G. Ceder, and U. V. Waghmare, Phys. Rev. Lett. **80**, 4911 (1998).
[44] G. D. Garbulsky, Ph.D. thesis, Massachusetts Institute of Technology, Cambridge, 1996.